SOFT ROBOTS

3D-printed programmable tensegrity for soft robotics

Hajun Lee[1], Yeonwoo Jang[1], Jun Kyu Choe[1], Suwoo Lee[1], Hyeonseo Song[1], Jin Pyo Lee[1], Nasreena Lone[1], Jiyun Kim[1,2]*

Tensegrity structures provide both structural integrity and flexibility through the combination of stiff struts and a network of flexible tendons. These structures exhibit useful properties: high stiffness-to-mass ratio, controllability, reliability, structural flexibility, and large deployment. The integration of smart materials into tensegrity structures would provide additional functionality and may improve existing properties. However, manufacturing approaches that generate multimaterial parts with intricate three-dimensional (3D) shapes suitable for such tensegrities are rare. Furthermore, the structural complexity of tensegrity systems fabricated through conventional means is generally limited because these systems often require manual assembly. Here, we report a simple approach to fabricate tensegrity structures made of smart materials using 3D printing combined with sacrificial molding. Tensegrity structures consisting of monolithic tendon networks based on smart materials supported by struts could be realized without an additional post-assembly process using our approach. By printing tensegrity with coordinated soft and stiff elements, we could use design parameters (such as geometry, topology, density, coordination number, and complexity) to program system-level mechanics in a soft structure. Last, we demonstrated a tensegrity robot capable of walking in any direction and several tensegrity actuators by leveraging smart tendons with magnetic functionality and the programmed mechanics of tensegrity structures. The physical realization of complex tensegrity metamaterials with programmable mechanical components can pave the way toward more algorithmic designs of 3D soft machines.

INTRODUCTION

Successful designs of soft robots rely on both clever morphology and material properties. Many researchers have pursued the intelligent embodiment of smart materials into the soft systems, which results in the dynamic interaction of architecture, material, and environment (*1*–*6*). However, body designs of soft robots have lagged behind biological analogs because of the inherent complexities in both form and function in generating suitable environmental behaviors at desired scales. Many different types of stimuli-responsive materials have been developed to add reversible and adaptive properties to artificial systems by transforming one form of energy into another (*7*–*16*). However, programmed responses of most smart materials depend largely on their intrinsic molecular or compositional structures. Consequently, recent developments in smart materials have advanced additional features, namely, the integration of multiple materials into a smart structure that can perform systematic functions resulting from structural traits and material and even share some common traits with living organisms (*2*, *8*, *16*). Full exploitation of the potential of soft actuators, therefore, necessitates alternative design principles and simple manufacturing routes capable of generating multimaterial parts with intricate three-dimensional (3D) architectures.

Structural approaches are essential to increasing the systematic complexity and the functional diversity of soft material–based intelligent systems. Smart structures can represent unconventional but programmable mechanical properties, reacting to environmental changes in morphologically and functionally adaptive ways (*17*, *18*). These features distinguish smart structures from typical static structures with a primary purpose of providing load capacity. In this context, metamaterial approaches have been widely used to aid additive manufacturing techniques (*19*). Flexible metamaterials—including auxetics (*20*–*23*), buckling (*24*–*27*), multistable structures (*28*, *29*), origami (*16*, *30*–*32*), and reinforced anisotropic systems (*33*)—emerging from mechanical properties governed by structure rather than composition have been designed to show diverse functionalities, such as programmable shape transformation, tunable mechanical properties, and energy absorption. For example, origami, and recently 4D printing, combines the use of additive manufacturing to produce free-form components with stimuli-responsive materials so that a printed 2D planar figure can transform into a programmed 3D morphology that responds to an external trigger (*16*, *34*–*36*). These printed structures usually show diverse morphing because of continuous or gradated material properties or hierarchical transformation with discrete arrangements of static links and functional joints (*37*, *38*). However, in most smart structures, most loads are focused on the flexible joints or hinges, and thus, combining multiple materials has limited synergistic effects in programming system-level mechanics to include both morphology and structural mechanics efficiently (*20*, *26*, *31*).

Therefore, to increase programmable complexity and synergistic integration in 3D, more scalable and systematic approaches should be promoted because of combinatorial issues brought about by embedding multiple distinct materials in a seamless and synergistic way. In addition, the interaction of a soft system with its surroundings ultimately depends on system-level mechanics, not only the bulk mechanics of the component materials. Exploiting such structural principles in advanced soft systems may lead to advances in design and manufacturing of future intelligent machines. The morphology, architecture, and mechanics of soft robots can be enhanced by exploring the ample design space offered by flexible metamaterials and devising manufacturing technologies that enable their physical realization.

We propose the adoption of tensegrity as a class of metamaterial strategy for smart material-based robotic systems. Tensegrity systems

[1]School of Material Science and Engineering, Ulsan National Institute of Science and Technology, Ulsan 44919, South Korea. [2]Center for Multidimensional Programmable Matter, Ulsan National Institute of Science and Technology, Ulsan 44919, South Korea.
*Corresponding author. Email: jiyunkim@unist.ac.kr

are composed of both isolated compressive "struts" and a network of elastic "tendons" with a specific configuration of nodes. Struts form a discontinuous system of members under compression that are surrounded by a continuous system of flexible elements (*39*–*41*). Since the term tensegrity was coined by Buckminster Fuller in the 1960s (*42*, *43*), tensegrity structures have been found in a diverse range of living organisms at every scale from intracellular structures (*44*–*46*) to human biomechanics (*47*, *48*). For example, the most primitive living things (like microorganisms) can adapt their shape and respond to their environment by exploiting both soft and stiff structures within their complex body plans, representing dynamic structural properties beyond their material properties (*46*, *49*). All vertebrates also maintain their structural solidity while retaining flexibility by networking stiff skeletal bones with tensile muscles (*48*).

The main advantages of tensegrity structures include high stiffness-to-mass ratio, controllability, reliability, structural flexibility, and large deployment (fig. S1). Furthermore, by preserving the self-equilibrium of normal forces applied to its elements, tensegrities are easily stabilized as the structure stands or is deformed. All internal stresses caused by deformation can be distributed throughout the entire structure, unlike other structural principles. One can control their static and dynamic characteristics by coordinating and adjusting compressive and tensional forces. In addition, tensegrity usually refers to beam-based structures, but any 2D or 3D components can be arranged into a tensegrity structure by balancing their compressive and tensile forces. This harmonious balancing of forces enables distinctive material components to be formed in a network, instead of piling up simple cellular units, and thus provides ample design space of morphology and mechanical properties. Because of this structural potential, most of the tensegrity studies have been conducted in the fields of art (*50*, *51*), toys, architecture (tents, bridges, etc.) (*52*–*55*), robotics for space application and exploration (*56*–*58*), and biomechanics (*59*, *60*). More frequently, tensegrities have been theoretically simulated using metamaterials or mathematically analyzed as a part of a mechanical system (*53*, *61*–*64*).

Despite its advantages, smart materials are rarely used as mechanical elements for the construction of smart tensegrity structures because of a lack of proper manufacturing processes. In several previous studies, smart materials such as shape memory materials and liquid crystal polymers were used for struts or tendons to achieve reconfigurable deployment of tensegrity structures or to trigger rolling of the tensegrity structures (*65*–*69*). However, their structural complexity has been limited because conventional tensegrity construction requires manual assembly of stiff struts and tensile components. Recently, both tendons and struts were 3D-printed to build tensegrity soft robots that exhibit simple motions (*68*–*71*), but printed parts still required manual assembly after the components were printed. In terms of the motional complexity, most tensegrity robots are designed on the basis of simple polygonal unit such as tetrahedron or icosahedron, demonstrating limited vibrational crawling, tumbling, or bending of the entire structure. Therefore, physical actualization of tensegrity systems combined with smart materials has been hindered by a lack of simple manufacturing routes that generate multimaterial parts with intricate 3D shapes. Consequently, this realization of diverse tensegrity designs with a proper design scheme will provide ample opportunities to explore the structure-level mechanics of tensegrity for soft robotic systems.

RESULTS

3D printing of tensegrity

We devised a simple process to 3D print tensegrity structures made of smart materials without requiring any additional assembly. Here, tensegrity structures consisting of monolithic tendon networks supported by struts were fabricated using 3D printing combined with sacrificial molding as shown in Fig. 1A. Commercialized 3D printers with dual printheads were used to print two structures simultaneously: A sacrificial mold with an internal channel network for injection of tendon material was printed with polyvinyl alcohol (PVA), and struts were printed with polylactic acid (PLA). After the entire structure was printed, polymeric smart materials in its liquid state were injected into the sacrificial mold. Then, we polymerized the tendon by applying heat and placed the structure in water to dissolve the sacrificial PVA mold. The diameters of tendon and strut range from 500 μm to 2 mm (fig. S2).

As a result, we could fabricate smart complex tensegrities with different topologies at diverse scales. Moreover, any material that can be injected into the channel of a sacrificial mold and polymerized under the remote stimuli can be used as a tendon (fig. S3). Our process allows us to fully exploit the potential of tensegrity for soft robotic applications through seamless digital integration of multiple distinctive materials via 3D printing.

The choice of soft materials for the tensile component is important in the design of soft robotic structures, because the stimuli-responsive actuation of tensegrity depends on the smart function and the mechanical properties of tendons. We used a soft magnetic composite material as the smart tensile component (tendon) in the tensegrity structure because it can be controlled remotely and operated rapidly in many media (*72*–*75*). Specifically, the use of magnetic fields as an actuation method obviates the need for direct contact in operating soft machines (*74*, *75*). We chose silicone-based elastomers—such as polydimethylsiloxane (PDMS), Ecoflex, and a mixture of these two—as base materials and mixed them with iron oxide (Fe_3O_4) magnetic microparticles to give magnetic functionality. Here, the magnetic composite tendon had 420 kPa of elastic modulus by mixing PDMS and Ecoflex in a 2:8 ratio with 30 weight % (wt %) of magnetic particles.

Design of tensegrity structure

In Fig. 2, we select a polygonal prismatic tensegrity unit and propose a design rule to build cylindrical tensegrity towers by assembling these units. This type of prismatic tensegrity unit has various configurations according to the base polygon (fig. S4), and here, we chose hexagonal prismatic tensegrity unit composed of a tendon network supported by separate struts as shown in Fig. 2A. We define a cylinder circumscribing the hexagonal prism tensegrity with the radius of R. The angle α measures the twisting between the two parallel base faces of the twisted prism, and *h* represents height of prism. In this case, the cylinder has 10-mm radius and 10-mm height. Struts and tendons have 2- and 1.5-mm diameter, respectively.

When we design a polygonal prismatic tensegrity unit, a cylindrical cavity inscribed by the arranged struts is created in the center of the tensegrity structure, as shown in Fig. 2B. The radius of the cylindrical cavity, r, can be easily calculated from the twisting angle, α, of the prism as follows: $r = |R\cos(\alpha/2)|$. The radius of the cavity decreases as α increases because each strut is a straight connection between two twisted nodes (Fig. 2B). The volumetric capacity of cylindrical tensegrity can be changed by changing the twisting angle,

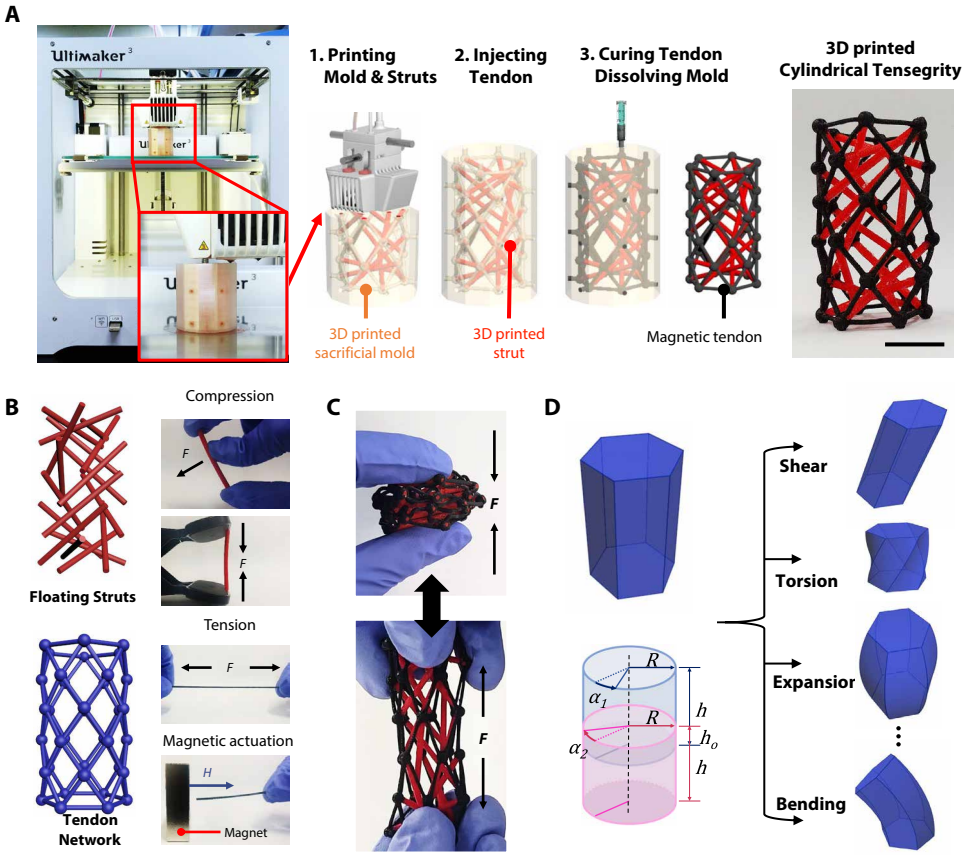

Fig. 1. Fabrication process of the tensegrity structure and mechanical features of its elements. (**A**) Fabrication process of the tensegrity structure through 3D printing technique and sacrificial mold technique. The picture on the left side shows dual material FDM (fused deposition modeling) printing of sacrificial mold with embedded struts. Schematic shows after printing process including material composite (MC) injection, thermal polymerization of MC, and dissolving sacrificial mold. The picture on the right side shows tensegrity structure obtained as a final product. (**B**) Elementary components of tensegrity: The tensional element, called a tendon, is a flexible magnetic composite containing magnetic particles in elastomer. Tendons are connected as a tensile network. The compressive element, called a strut, is printed PLA fiber. They are disconnected from each other and support the tendon network at all nodes (movie S1). (**C**) Large deployment of cylindrical tensegrity induced by passive contact forces. (**D**) Schematics of transformations of tensegrity beams decided by design parameters. Scale bar, 10 mm.

α (fig. S5). This prismatic unit tensegrity shows contraction accompanied with torsion with zero Poisson's ratio when axial compressive force is applied to the structure because of the twisted arrangement of struts, as shown in Fig. 2C. The structure rotates until the tilting struts meet, and the direction of rotation corresponds to the twisting angle, α. Torsional angle decreases as α increases, because the twisting angle itself already matches the rotatable angle of struts. The elastic modulus also decreases as α increases because the struts with large twisting angles are already tilted, having low resistance to bear the compressive load (fig. S6).

The twisted prisms are vertically coordinated to build the tower tensegrity (fig. S7). How these polygonal prism tensegrities are assembled into a cylindrical structure decides the structure-level mechanics of the resulting tensegrity tower. Several possible compositions of the geometry of a tensegrity tower are shown in Fig. 2D. When two twisted prisms are aligned vertically with an overlapping rate of height, h_o, the angle α measures the twisting of a twisted prism unit as we already defined, and β is the relative rotation between the two prism layers. By altering α, β, h, and h_o, as well as the base polygon of the twisted prisms, we can design diverse cylindrical tensegrity tower structures.

For example, we observed the mechanical responses of a five-layered cylindrical tensegrity tower obtained from the hexagonal prisms with α = 90°, β = 0°, and h_o = 0%, as shown in Fig. 2 (E to H). Each layer has a height of 10 mm, and consequently, the tensegrity tower becomes 50 mm tall. According to the types of forces, the structure shows three different deformations: contraction with torsion, elongation with torsion, and bending. If the compressive force is applied to the structure in an axial direction, it shows the contraction with zero Poisson's ratio (fig. S8) accompanied with the torsion (Fig. 2F), and the twisting angle is linearly proportional to the strain (Fig. 2I). Rotating angle of this tensegrity depends on the twisting angle of a unit prism, resulting in the counterclockwise rotation in this case. On the other hand, when the pulling force is applied in the axial direction, the structure expands, rotating in the reverse direction (Fig. 2, G and J). Furthermore, this tensegrity tower is able to bend when the eccentric compressive force is applied to one node of the base hexagon (Fig. 2H), and the bending angle increases as the applied load increases, as shown in Fig. 2K.

Programming structure-level mechanics

A free choice of the geometrical parameters leads to diverse tensegrity structures. By altering α, β, h, and h_o, as well as the base polygon of the twisted prisms, here, we present several types of cylindrical tower tensegrities with programmed structure-level mechanics—such as stiff response under the axial compression, transverse expansion with little contraction under torsional shear, axial contraction with zero Poisson's ratio with programmable rotating angle, and linear shear strain under the shear stress—in Fig. 3. Finite element method with ABAQUS was used to numerically simulate the deformation of individual cylindrical tensegrities under the specific stresses. All results correspond well to the transformation of all tensegrities.

Specifically, a tensegrity tower based on hexagonal prisms with α = 180°, β = 0°, and h_o = 0% becomes a stiff structure whose mechanical properties depend substantially on the struts and their arrangement, because struts are vertically connected with each other throughout all layers in this configuration (Fig. 3A). When the axial compressive force is applied, it shows little contraction compared with other flexible tensegrity structures. Their stress-strain behaviors vary according to the twisting angle, α, of a unit hexagonal

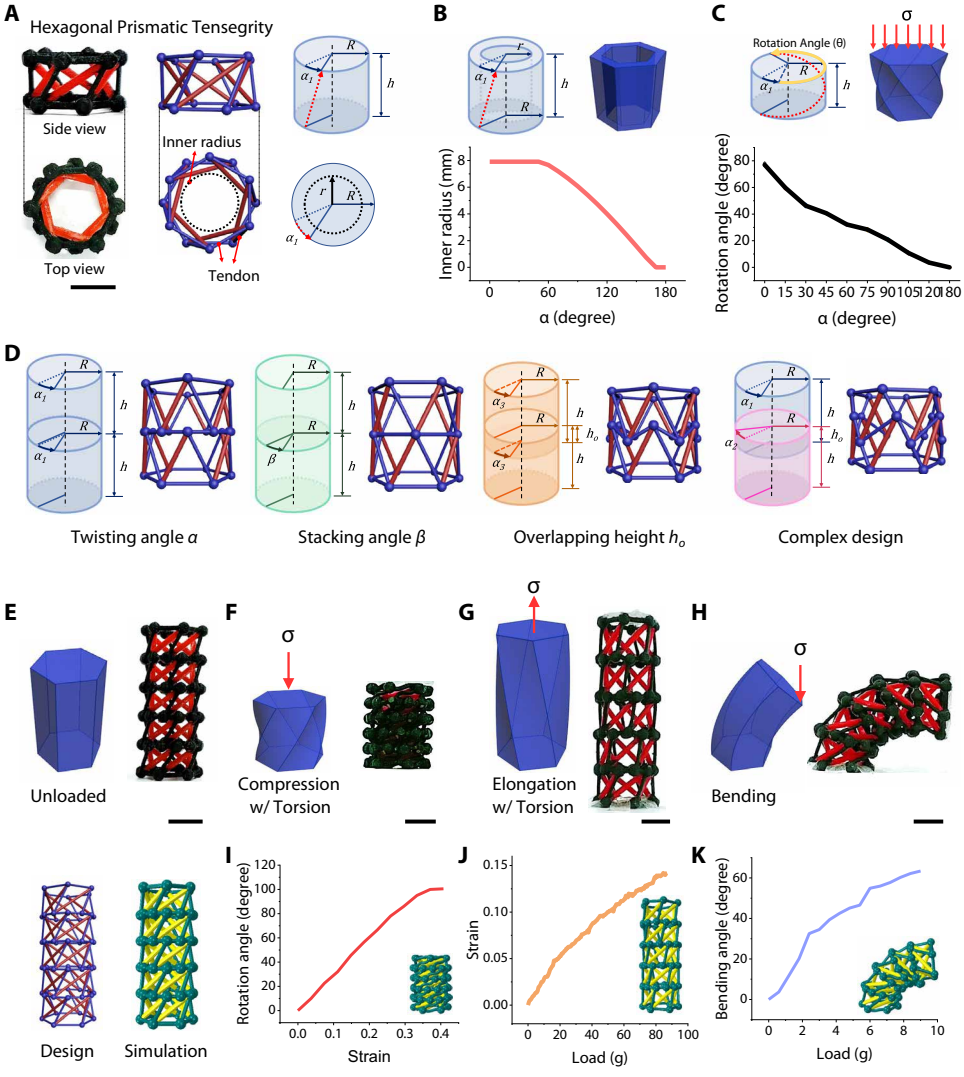

Fig. 2. Design parameters of tensegrity structure and controllable mechanical properties using design parameters. (**A**) Geometry of a single tensegrity unit of α = 90°, the twisting angle between ceiling and ground of the single unit, on side view and top view. (**B**) Radius of interior space according to the angle of α in the range of 0° to 180°. (**C**) Rotational angle of the single unit by compressive force according to the angle of α in the range of 0° to 120° and additional 180°. (**D**) Three design parameters—twisting angle, α; stacking angle, β; and overlapping height, h_o—in a tensegrity beam. The example designs and the complex design were fabricated by applying multiple design parameters at the same time. (**E**) Schematic image, picture, geometric design, and simulation graphic of the tensegrity beam at an unloaded state without deformation. Design parameters are α = 90°, β = 0°, and h_o = 0. (**F**) Schematic image and the contraction of the cylindrical tensegrity accompanied by torsion under the axial compression. (**G**) Schematic image and extension of the cylindrical tensegrity accompanied by torsion in reverse direction under the axial tension. (**H**) Schematic image and the bending of the cylindrical tensegrity. (**I**) Rotational angle according to the longitudinal strain under the axial compression and its simulation result. (**J**) Longitudinal strain according to load under the tension and its simulation result. (**K**) Bending angle according to load during bending and its simulation result. Scale bars, 10 mm.

prism as the configuration of the strut network changes as shown in Fig. 3B. This type of tensegrity tower becomes stiffer as the twisting angle α increases because the struts are overlapped with each other even in a layer, increasing their mechanical strength.

In case of the tensegrity tower with design parameters of α = 60°, β = 0°, and h_o = 50%, the struts are partially connected with each other (struts throughout one to three layers and two to four layers in this case). Here, the height of a unit hexagonal prism is 2*h* to maintain the height of the tensegrity tower with other cases. In this configuration, when the torsional shear stress is applied to the structure, the tensegrity expands in the lateral direction, as shown in Fig. 3C, with little tensile strain. Their transverse expansion strain according to the rotating angle is displayed in Fig. 3D.

In addition, the rotation angle of a cylindrical tensegrity tower can be programmed by designing how different types of hexagonal prisms are assembled. For example, as shown in Fig. 3E, we alternately assembled two different hexagonal prism tensegrities with α = 90° and −90°, β = 0°, and h_o = 0%. When the compressive force is applied to the tensegrity tower, the twisting of a prismatic tensegrity unit can be cancelled by the inverse rotation of the other prismatic tensegrity layer that has an opposite twisting angle, α. Consequently, the torsions of unpaired units only remain after the complete contraction as shown in Fig. 3F.

The last type of mechanical response is linear transverse shear movement, which is found in the tensegrity tower structure with design parameters of α = 0°, β = 0°, and h_o = 0%. Struts are connected in a vertical direction without tilting, which makes this structure resistive to the compressive axial stress but compliant to the shear stress (movie S2).

Magnetic actuation of tensegrity structures

In Fig. 4, we designed diverse tensegrity structures based on triangular prismatic tensegrity (Fig. 4A), including the icosahedron tensegrity that is one of the mostly used tensegrity structures in robotic applications, the auxetic tensegrity into which the triangular prisms are assembled in the horizontal direction, and the cylindrical tensegrity tower whose cross-sectional area is narrowed down. All the base polymer composites of tendon network contain 30 wt % of magnetic particles. Thus, all these magnetic tensegrity actuators quickly deform within 0.5 s according to their programmed mechanical characteristics under the applied magnetic field due to the magnetic force F = ∇(m·B) between the magnet and the structure, and rapidly recover their original shape upon removal of the applied magnetic field.

First, icosahedron-based tensegrity structures composed of 6 PLA struts and 24 composite tendons were investigated as shown

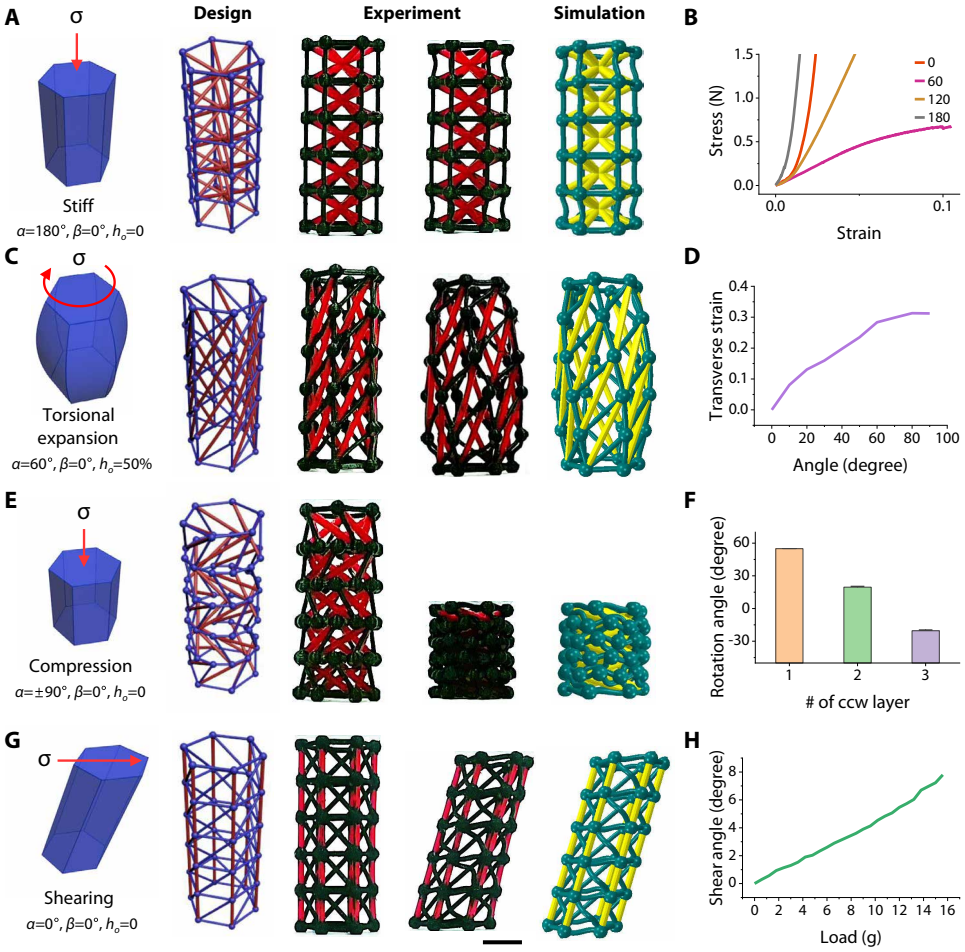

Fig. 3. Transformation and mechanical properties of cylindrical tower tensegrity structures with different design parameters. (**A**) Schematic of mechanical response types, geometric design, picture of deformation, and simulation result of the stiff tensegrity beam. Design parameters are $\alpha = 180°$, $\beta = 0°$, and $h_o = 0$. (**B**) Stress-strain curves of stiff tensegrities with different α (0°, 60°, 120°, and 180°) and the same β and h_o as 0. (**C**) Schematic of mechanical response type, geometric design, picture of deformation, and simulation result of the cylindrical tensegrity showing transverse expansion under the torsion with little contraction. Design parameters are $\alpha = 60°$, $\beta = 0°$, and $h_o = 50\%$. (**D**) Transverse strain according to torsional angle of the tensegrity in (C). (**E**) Schematic of mechanical response type, geometric design, picture of deformation, and simulation result of the cylindrical tensegrity with programmable rotation angle under the compression. Design parameters are α = alternating ±90°, $\beta = 0°$, and $h_o = 0$. (**F**) Total rotation angle according to the arrangement of prismatic units with opposite twisting angle α in clockwise (cw) or counterclockwise (ccw) direction. (**G**) Schematic of mechanical response type, geometric design, picture of deformation, and simulation result of the cylindrical tensegrity resistive to compression but compliant to shear. Design parameters are $\alpha = 0°$, $\beta = 0°$, and $h_o = 0$. (**H**) Shear angle according to the applied load in (G). Scale bar, 10 mm.

are elastomeric composite tendons and stiff PLA struts. Regardless of the tendon's elastic modulus, all tensegrities can maintain their structure with the aid of stiff struts supporting the tendon network. However, magnetic deployment increases as the elastic modulus of the tendon decreases under the same magnetic field because composite tendons provide additional tensional forces to withstand the structure while the structure deforms.

These results show that the mechanical stiffness of individual compressive or tensional components can affect the overall flexibility of tensegrity; however, we can enhance the structural solidity that elastomer networks cannot provide by synergistically arranging both functional soft tendons and supporting stiff struts in tensegrity architecture. First, icosahedron tensegrity was only composed of flexible elements. The elastic modulus of tendons was changed by controlling the mixing ratio of two silicone-based elastomers: PDMS and Ecoflex. As shown in Fig. 4B, icosahedron-based tendon networks composed only of an Ecoflex composite (i.e., having the lowest elastic modulus among our composites) cannot maintain the structure as designed even without the application of an external magnetic field. When the magnetic field was applied, this Ecoflex-based tendon network completely collapsed. Therefore, the structural integrity of single-material elastomeric networks crucially depends on the mechanical properties of the material (fig. S10 and movie S3).

We also demonstrated a planar auxetic tensegrity assembled with triangular prismatic tensegrity units (α = 0°) in horizontal direction (Fig. 4C). This structure is composed of vertically arranged struts and two layers of auxetic tendon networks combining these struts. The diameter and height of the auxetic tensegrity were 70 and 20 mm, respectively. The actuator could exhibit auxetic behavior upon the application of an external magnetic field (movie S4). When we applied remote vertical compressive force using a magnetic field in the middle of the tensegrity plane, the upper layer of the tendon network exhibited shrinkage toward the center of this actuator. When we slid the magnet under the actuator, applying a weaker magnetic field, the tendon layer created complex undulating patterns showing auxetic behaviors.

Figure 4D represents a starfish-shaped tensegrity structure composed of five tensegrity tower legs. Each leg has design parameters of α = 60°, β = 30°, and h_o = 50%. To mimic the shape of starfish's

in Fig. 4B. All icosahedron tensegrities are about 28 mm in overall size and have 1.5 mm in diameter of tendon elements. In addition to the structural configuration, the material composition of tensegrity is another major factor that determines the intensity of mechanical responses (fig. S9). Thus, we compared the magnetic deployment of icosahedron tensegrities with different material compositions for both tendon and strut. The deployment was defined by height difference of icosahedron tensegrities before and after a remote compressive force was applied to the structure using the external magnetic field from a permanent magnet. The effect of material composition on magnetic deployment of the structure becomes more obvious when this tensegrity is composed of two distinctive materials, which

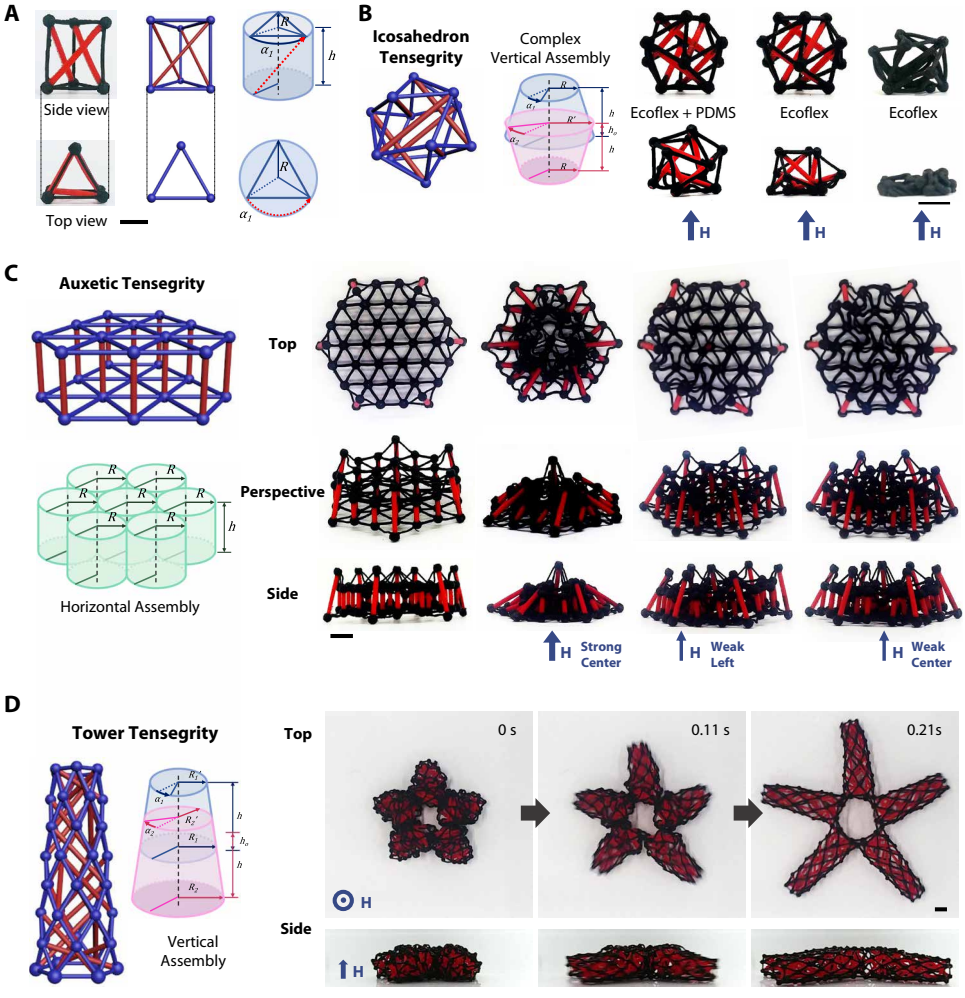

Fig. 4. Various magnetic actuation of tensegrity structures. (**A**) Triangular prismatic tensegrity structure as a unit. (**B**) Icosahedron-based tensegrity structure composed of two modified triangular prismatic tensegrity units. The design parameters are $\alpha = \pm 60°$ for top and bottom, $\beta = 30°$, and $h_o = 36.7\%$. The radius of the intersection R' is equal to $1.62R$. Comparison of magnetic deployment of icosahedron tensegrity structures with different material composition. Degree of deployment can be changed by the material, in addition to the structure. (**C**) Design rule of an auxetic tensegrity actuator. Magnetic deployment and auxetic behaviors upon the application of an external magnetic field. Top views, oblique views, and side views of auxetic tensegrity and its actuations are represented. (**D**) Starfish-shaped tensegrity structure composed of vertically assembled tensegrity beams with gradually narrowed cross-sectional area and its rapid structure restoration from full contraction within 0.5 s. Scale bars, 10 mm.

leg, the cross-sectional area of each leg was gradually narrowed down. The cross-sectional diameter of each leg was about 25 mm, and it narrowed to about 15 mm at the outer end of each leg. The overall size of the tensegrity tower was about 153 mm. Each leg of this starfish-shaped tensegrity actuator was able to contract; the structure showed large deployment along the axial direction of each leg rather than along the radial direction. As shown in Fig. 4D, this tensegrity maintained their anisotropic deformation under the magnetic field and rapidly recovered their original shape when the external magnetic field was removed. In addition to the simple polygonal prismatic tensegrity unit, many other tensegrities units can be designed to have specific mechanical responses (figs. S11 to S13 and movie S5). These units can be assembled into large superlattices, and their mechanical responses and the corresponding magnetic actuation can be programmed according to their arrangement and connectivity (figs. S14 to S18 and movie S6). In addition, to show that our design principle can be successfully applied to program both morphology and mechanics of soft structure in an independent manner, we demonstrated diverse morphologies of tensegrity structures with programmed mechanical property in fig. S19. By arranging aperiodic units, cylinder-, arch-, pyramid-, and sphere-shaped tensegrities have distinctive morphologies but with the same torsional compression.

Composite-handed toroidal tensegrity structure

We also composed a toroidal tensegrity structure, assembling four tensegrity units: two cylindrical tensegrity units for the compliant parts and two bent cylindrical tensegrity units for the stiff parts (Fig. 5A). The toroidal tensegrity loop is 30 cm long with 2 cm of outer diameter and composed of 30 layers of hexagonal prismatic tensegrities. Nine-layered cylindrical tensegrity units with different rotational directions under the compression were adopted as compliant parts, and stiff tensegrities were used at each round side of the loop to connect two compliant tensegrities. The compliant tensegrities have the design parameter of $\alpha = 60°$ for right-handed arrangement of strut and $\alpha = -60°$ for left-handed arrangement of struts, and others are the same as $\beta = 0°$ and $h_o = 0\%$. Stiff tensegrities have the parameters with $\alpha = \pm 60°$, $\beta = 30°$, and $h_o = 0\%$. As shown in Fig. 5B, right-handed tensegrity contracts under counterclockwise torsional shearing and expands under clockwise torsional shearing. On the contrary, left-handed tensegrity contracts under the clockwise torsional shearing and extends under the counterclockwise torsional shearing.

According to the composition of the toroidal tensegrity unit with cylindrical tensegrity units with different handedness in strut arrangements, their deformation patterns were demonstrated as shown in Fig. 5C. In the toroidal tensegrity unit with homogeneous handedness, compliant sides were composed of cylindrical tensegrity units having the same rotational direction. On the other hand, the toroidal tensegrity with heterogeneous handedness was made of cylindrical tensegrity units with opposite rotational directions. When we applied the same types of forces to each structure, they showed different deformation patterns because of different handedness. For example, when we twisted the toroidal tensegrity composed of only right-handed cylindrical tensegrity units, they contracted or elongated at the same time because all compliant parts rotated in the same direction. Thus, the twisted eight-like structure contracts or

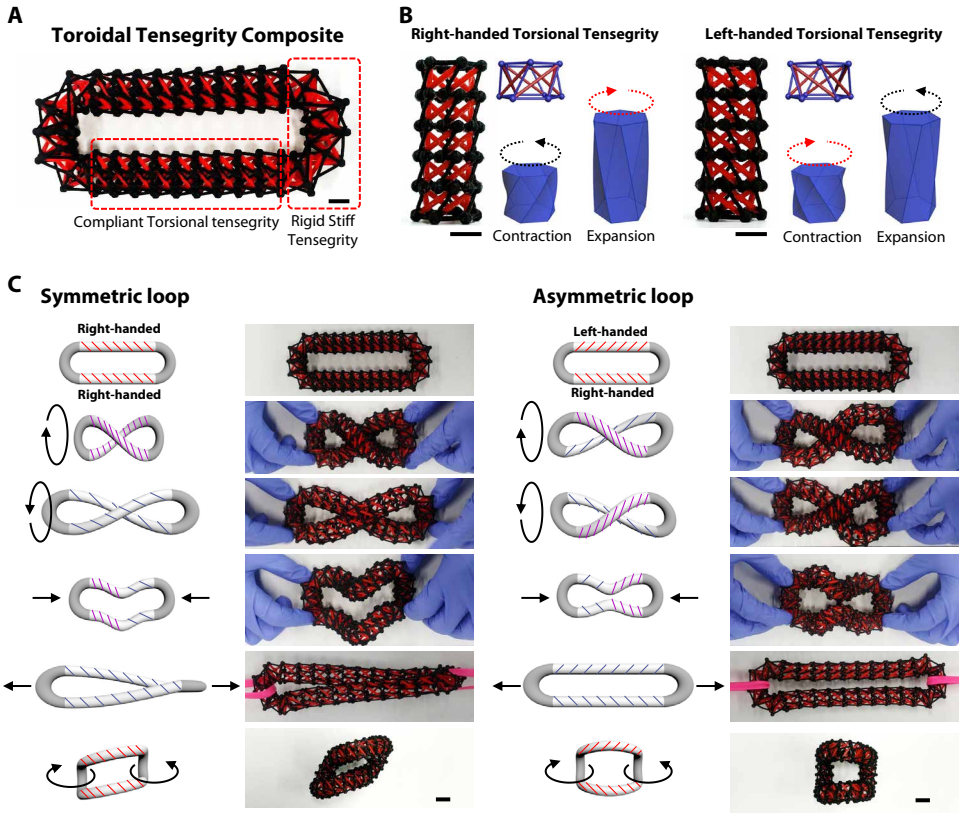

Fig. 5. Various transformations according to the handedness of the toroidal tensegrity loop. (**A**) Toroidal tensegrity composite consisting of two types of tensegrity structures: compliant torsional tensegrity and stiff tensegrity. The design parameters of stiff part are as follows: $\alpha = 90°$ on a half side and $-90°$ on the other half, $\beta = 30°$, and $h_o = 0$. (**B**) Compliant cylindrical tensegrity beams with opposite handedness. Left one is a right-handed torsional tensegrity, the same one presented in Fig. 2E, and the other is a left-handed torsional tensegrity. Schematics show unit designs and rotational directions according to contraction and expansion. (**C**) Schematics and pictures of transformation of symmetric and asymmetric loops according to external forces in various directions: (from the top) unforced, torsion, compression, elongation, and bending. Scale bars, 10 mm.

expands according to the twisting direction. On the other hand, when we twisted the toroidal tensegrity composed of right-handed and left-handed cylindrical tensegrity units at each side, a cylindrical tensegrity expanded when the other one contracted and vice versa. Consequently, the twisted eight-like structures maintain the same size and shape (no difference in its total length) because one side expands when the other contracts regardless of the twisting direction of the torsional shearing force. Other deformation patterns under the different types of external forces are also different according to the handedness of cylindrical tensegrity units as shown in Fig. 5C. Additional heterogeneous assembly of cylindrical tensegrity units and the differences in their transformations were demonstrated in fig. S20.

Starfish-shaped walking tensegrity robot

Here, we develop a starfish-shaped walking tensegrity robot with five legs made of cylindrical tensegrity tower structures (Fig. 6A). This tensegrity structure is composed of alternating layers of hexagonal prisms with the design parameters of $\alpha = \pm 90°$, $\beta = 0°$, and $h_o = 0\%$, thus showing little twisting under the axial compression and compliantly bends under the eccentric compression. Two small motors were mounted on each leg to bend and contract the leg independently. As shown in Fig. 6B, when both motors do not wind the threads, the tensegrity leg is relaxed without any deformation. On the other hand, the leg is linearly contracted when the top motor axially pulls the structure winding the thread, and the leg compliantly bends when bottom motor applies eccentric compressive force winding the thread. By winding and unwinding the threads of each leg, we were able to create sequential motions for the forward locomotion of the tensegrity robot. Specifically, two front legs were chosen to drag the body forward by bending the legs from the relaxed state, and simultaneously, one rear leg pushes the body by extending the leg from the bended state to assist the forward movement. Although three legs are walking, the remaining side legs maintain the contraction so as not to disturb the walking sequence. Consequently, the robot can change the direction of movement simply by operating different front and rear legs, as shown in Fig. 6 (C and D). More detailed information about the robot anatomy, control circuits, and operation is provided in fig. S21 (movie S7).

DISCUSSION

In this work, we adopted the tensegrity for the development of soft structures with programmable mechanical responses in 3D. Tensegrity structures are composed of flexible elements and stiff elements—so-called tendons and struts, respectively—and share characteristics such as lightweight construction, small volume occupancy, and high flexibility. Thus, tensegrity provides essential rules for constructing programmable architectures that have both structural integrity and flexibility. We endowed tensegrity with additional functionality by using magnetic materials as tendon components and used a 3D printing technology combined with sacrificial molding to fabricate tensegrities at a diverse scale. This method makes the construction of tensegrity a lot easier because it eliminates any post-assembly process of beam elements.

As a result of printing tensegrity with coordinated soft and stiff elements, we could use design parameters (such as geometry, topology, density, coordination number, and complexity) to program structure-level mechanics in a soft structure. On the basis of the programmed mechanics of tensegrity structures, we developed diverse smart structures and demonstrated a tensegrity robot capable of walking in any direction. We demonstrated several tensegrity actuators (such as auxetic behavior, locomotion, and intaking) by leveraging smart tendons with magnetic functionality. This physical realization of complex 3D metamaterials with multiple mechanical components can pave the way toward more analytical and algorithmic designs of scalable geometry and contribute to complex morphing

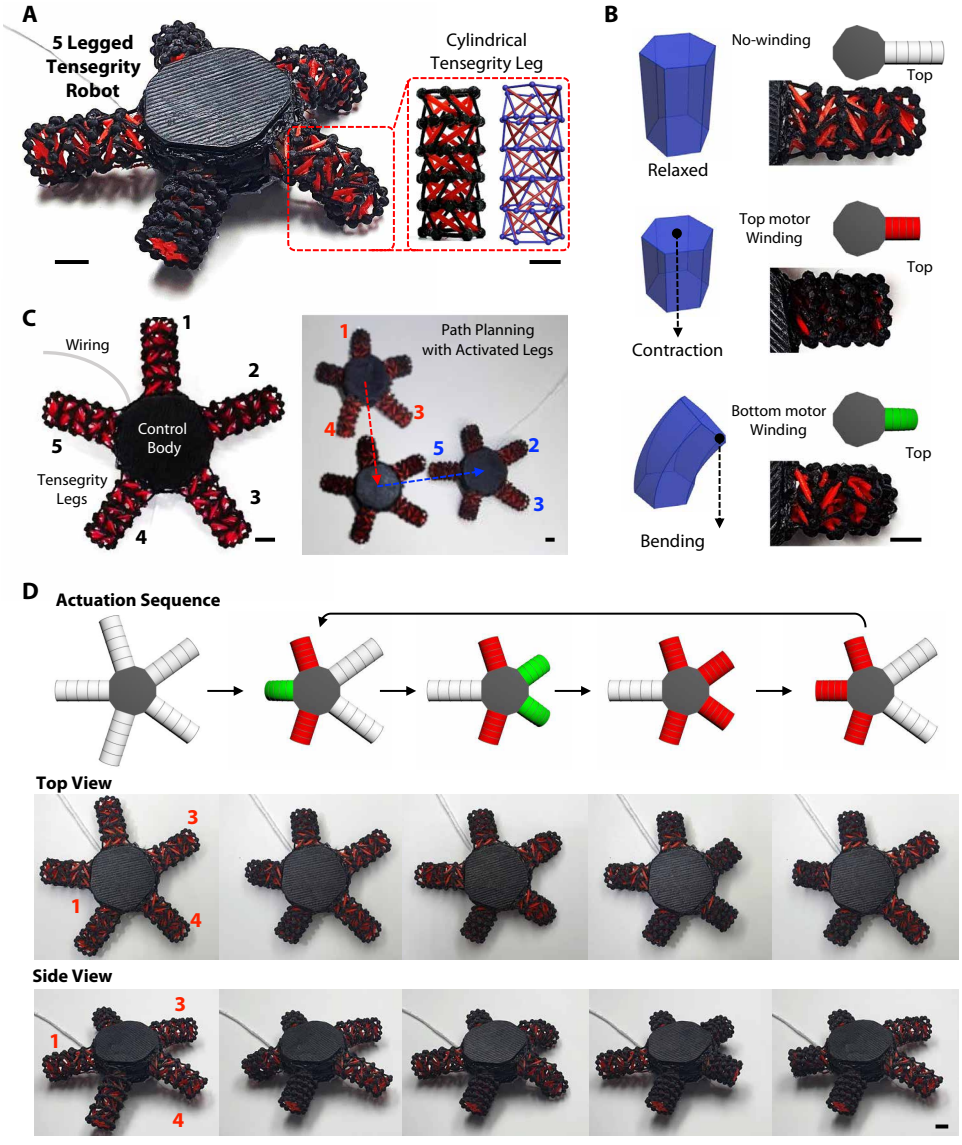

Fig. 6. Multidirectional locomotion of starfish robot. (**A**) Starfish robot with five identical legs composed of cylindrical tensegrity beam and 3D-printed body. Design parameters of each leg are the same as α = alternating ±90°, $\beta = 0°$, and $h_o = 0$. (**B**) Types of reversible transformations of a leg by installed motor on the body. On the left side, schematics of three transformation of the leg are presented, indicating the point at which the stress is applied. Pictures and schematics of each actuation are shown on the right side. Gray polygon describes the body, and colored cylinders indicate the leg in relaxation (white), contraction (red), and bending (green). (**C**) Trajectory of multidirectional locomotion of the starfish robot, turning right after moving down. The set of activated legs is changed from (1,3,4) to (2,3,5). (**D**) Sequence of walking of the starfish robot, from left to right. The locomotion of the starfish robot consists of repeating four sequences. (Top) Schematics of transformation states of each leg. (Middle) Pictures of top view. (Bottom) Pictures of side view. Scale bars, 10 mm.

for 3D soft systems. Furthermore, this may provide new form factors for 3D flexible devices in the fields of flexible electronics, biomedicine, and soft robotics.

MATERIALS AND METHODS

Design and 3D printing of strut and sacrificial mold

We used a 3D modeling tool (3DS MAX, AUTODESK Inc.) to design the sacrificial mold and an open-source slicing engine (Ultimaker Cura, Ultimaker B.V.) to convert stereolithography (STL) files of sacrificial mold into a g-cord format. The 3D printer that we used was Ultimaker 3 (Ultimaker B.V.). Printer cores of the Ultimaker 3 were a Core AA with a 0.25-mm-diameter nozzle for a PLA (Ultimaker B.V.) filament with a 2.85-mm diameter and a Core BB with a 0.40-mm-diameter nozzle for a PVA (Ultimaker B.V.) filament with a 2.85-mm diameter. A preset profile ("Fine – 0.1 mm," resolution of layer height is 0.1 mm and line width is 0.23 mm) of print settings was used with slight modifications: 10% infill density for PVA, 190°C default printing temperature for PLA, and disabled support generation.

Fabrication of tensegrity structure

PDMS (Sylgard 184, Dow Corning) and Ecoflex 00-30 (Smooth-on) were prepared for elastomeric components. Two prepolymers of PDMS were mixed at a ratio of 9:1, and two prepolymers of Ecoflex 00-30 were mixed at a ratio of 1:1. Their prepolymer mixtures were mixed together in ratios from 10:0 to 0:10 to change the mechanical stiffness of tendons, and 30 wt % magnetic particles (Fe_3O_4, 310069, Sigma-Aldrich) were added into mixed elastomer resin to fabricate magnetic composite tendon. After mixing all the components for 2 min, we degassed the composite resin under vacuum in a vacuum oven at room temperature for 5 min. A NORM-JECT syringe (Henke-Sass Wolf) without a needle was used to inject the magnetic composite resin into the channel of preprinted sacrificial mold. The entire printed structure with injected magnetic composite was wrapped with commercially available aluminum foil to prevent leakage of liquid composite, followed by curing on the hot plate set at 80°C over 6 hours. The aluminum foil was stripped away from the printed structure after the magnetic tendon network was polymerized and then the sacrificial mold was dissolved in the water chamber overnight. For fabrication of starfish robot, each leg was fabricated with the same method as other tensegrity structures. The body of the robot was designed via a 3D printer to withstand all the forces driven by each leg. Ten micro DC motors were placed in the body of the robot and at the bottom of the body. Each leg and pairs of the motors were connected by a fabric sewing thread.

Mechanical characterization of elastomeric components

We tested mechanical characterization of elastomeric components composed of various magnetic composites with different ratios of

PDMS and Ecoflex from 10:0 to 0:10. Samples were prepared as films of rectangular shape sized 75 mm × 11.5 mm × 1.3 mm (width × length × thickness), and the test was processed using a mechanical testing machine (AGX-100NX, SHIMADZU) at a strain rate of 50 mm/min. To obtain stress-strain curves of tensegrity structures with different design parameters, we conducted compressive tests. We placed samples on the 3D-printed rotating stage to offset the torsional factors as much as possible during compressive tests. They were processed using a mechanical testing machine (3343, INSTRON) at a compress rate of 50 mm/min. For the rotation angle, we marked the red dot on the rotating stage and tracked it during the compressive test. Elongation, bending angle, and tensile angle were measured by analyzing pictures of the tensegrity structure transformed by hanging weights on tensegrity beam fixed on the stage. Transverse strain was measured by same picture analyzation, but it was processed on the rotating stage (fig. S22).

Magnetic actuation of tensegrity structure

We used an NdFeB magnet of 60 mm × 50 mm × 15 mm (width × length × thickness), whose magnetic field intensity is 250 mT in the center of the surface of the permanent magnet. For the actuation of tensegrity structures, the magnet was manually controlled under the stage on which the tensegrity structures were placed, and the magnet was taken away from the stage for restoration of tensegrity structures. For expansion, bending, and locomotion of tensegrity structures, the magnet was manually manipulated along the intended path to actuate the tensegrity structure. To induce the propagating auxetic behavior of auxetic tensegrity actuators, we used another magnet, 50 mm × 10 mm × 5 mm (width × length × thickness), whose magnetic field intensity is 80 mT in the center of the surface of the permanent magnet.

Circuit for controlling starfish robot

To control the starfish robot, we used Arduino. Each of the motors was connected to Arduino and a power supply (PWS2326, TEKTRONIX) through H-bridges (L293D). The code for the operation of the actuations was completed using an integrated development environment (IDE), a software application. A computer with the saved code transferred the serial data into the input pins of the microcontroller. The processed data through the controller transmitted to the input pins in L293D, which is an H-bridge delivering bidirectional current. The output pins in L293D connected to motor wires received serial data from the input pins. A power supply should provide electric voltage from 5 to 6 V with the supply voltage pin in L293D due to the stable power for the motor.

Finite element analysis

Finite element analysis was implemented by the commercially available software ABAQUS to predict transformations of tensegrity beams with different design parameters under various types of external stress. A total of seven transformation types of tensegrity beams were simulated using tensegrity beams presented in Figs. 2 and 3. The models for the simulation were designed with a 3D modeling tool (Fusion 360, Autodesk Inc.). Two elements of tensegrity beam, tendon and strut, were designed separately and then they were selectively tied at each node. After that, the external stress was applied by a rigid plate above the tensegrity beam to transform it, to the direction appropriate for each type of transformation. The tendon network was constructed with the silicone rubber, Ecoflex 00-30, and its mechanical property was constituted using hyperelastic Arruda-Boyce material model with the following parameter values: $\mu = 0.03$, $\lambda_M = 3.9$, and $D = 0$. The strut was constructed with the PLA, and its mechanical property was an elastic model with the following parameter values: Young's modulus $E = 3500$ MPa and Poisson's = 0.36.

SUPPLEMENTARY MATERIALS

robotics.sciencemag.org/cgi/content/full/5/45/eaay9024/DC1

Fig. S1. Structural advantages of tensegrity compared other conventional structures.
Fig. S2. Fabrication of tensegrity structure.
Fig. S3. Tensegrity structures composed of diverse materials in a wide range of scales.
Fig. S4. Variation of volume fraction according to the structural complexity.
Fig. S5. Example designs of tensegrity beam and comparison of their inner spaces according to types of transformation.
Fig. S6. Stress-strain curve of single tensegrity unit according to α.
Fig. S7. Mechanical properties of tensegrity beam according to the number of layers.
Fig. S8. Mechanical properties of tensegrity beam according to the number of layers with opposite rotation direction.
Fig. S9. Mechanical properties of tensegrity structures according to material.
Fig. S10. Magnetic deployment according to existence of strut.
Fig. S11. Mechanical properties of tensegrity structures according to topology.
Fig. S12. Membrane tensegrity with 2D tendons.
Fig. S13. Particle uptake by rolling-based locomotion.
Fig. S14. Flexibility control of linear tensegrity lattice composed of tetrahedral tensegrity units according to connectivity of tendons.
Fig. S15. Structural flexibility depending on the density of tensegrity unit.
Fig. S16. Diverse arrangements of tensegrity unit and transformation.
Fig. S17. Large-scale superlattice consisted of IBT units.
Fig. S18. Large-scale superlattice consisted of CBT units.
Fig. S19. Torsional compression of tensegrity structures with diverse morphologies.
Fig. S20. Different transformation structure in the square loop structure according to transformation direction.
Fig. S21. Body and circuit design of the starfish robot.
Fig. S22. Compression test setup.
Data file S1. Zipped folder containing stereolithography (STL) files of 3D-printed molds and struts for diverse tensegrity structures used in this work: AT, CBT, CT, HPBT, BTPBT, IBT, and SST.
Movie S1. Mechanical response of tensegrity composed of tendon and struts.
Movie S2. Transformation types of tensegrity beam according to design parameters.
Movie S3. Mechanical anisotropy and integrity of tensegrity.
Movie S4. Magnetic actuations of auxetic tensegrity.
Movie S5. Rolling-based locomotion of CBT and CT actuators for particle uptake.
Movie S6. Programmed mechanical property of large-scale superlattice composed of different tensegrity unit.
Movie S7. Starfish robot actuation composed of five tensegrity legs.
Movie S8. Overview of 3D-printed programmable tensegrity.

REFERENCES AND NOTES

1. R. Pfeifer, J. C. Bongard, *How the Body Shapes the Way We Think: A New View on Intelligence* (MIT Press, 2006).
2. A. Rafsanjani, Y. Zhang, B. Liu, S. M. Rubinstein, K. Bertoldi, Kirigami skins make a simple soft actuator crawl. *Sci. Robot.* **3**, eaar7555 (2018).
3. S. Baik, D. W. Kim, Y. Park, T.-J. Lee, S. H. Bhang, C. Pang, A wet-tolerant adhesive patch inspired by protuberances in suction cups of octopi. *Nature* **546**, 396–400 (2017).
4. A. S. Gladman, E. A. Matsumoto, R. G. Nuzzo, L. Mahadevan, J. A. Lewis, Biomimetic 4D printing. *Nat. Mater.* **15**, 413–418 (2016).
5. B. Shin, J. Ha, M. Lee, K. Park, G. H. Park, T. H. Choi, K.-J. Cho, H.-Y. Kim, Hygrobot: A self-locomotive ratcheted actuator powered by environmental humidity. *Sci. Robot.* **3**, eaar2629 (2018).
6. T. Li, G. Li, Y. Liang, T. Cheng, J. Dai, X. Yang, B. Liu, Z. Zeng, Z. Huang, Y. Luo, T. Xie, W. Yang, Fast-moving soft electronic fish. *Sci. Adv.* **3**, e1602045 (2017).
7. L. Hines, K. Petersen, G. Z. Lum, M. Sitti, Soft actuators for small-scale robotics. *Adv. Mater.* **29**, 1603483 (2017).
8. S.-J. Park, M. Gazzola, K. S. Park, S. Park, V. D. Santo, E. L. Blevins, J. U. Lind, P. H. Campbell, S. Dauth, A. K. Capulli, F. S. Pasqualini, S. Ahn, A. Cho, H. Yuan, B. M. Maoz, R. Vijaykumar, J.-W. Choi, K. Deisseroth, G. V. Lauder, L. Mahadeva, K. K. Parker, Phototactic guidance of a tissue-engineered soft-robotic ray. *Science* **353**, 158–162 (2016).
9. M. Rogóż, H. Zeng, C. Xuan, D. S. Wiersma, P. Wasylczyk, Light-driven soft robot mimics caterpillar locomotion in natural scale. *Adv. Opt. Mater.* **4**, 1689–1694 (2016).
10. A. Miriyev, K. Stack, H. Lipson, Soft material for soft actuators. *Nat. Commun.* **8**, 596 (2017).

11. H. Arazoe, D. Miyajima, K. Akaike, F. Araoka, E. Sato, T. Hikima, M. Kawamoto, T. Aida, An autonomous actuator driven by fluctuations in ambient humidity. *Nat. Mater.* **15**, 1084–1089 (2016).
12. W. Hu, G. Z. Lum, M. Mastrangeli, M. Sitti, Small-scale soft-bodied robot with multimodal locomotion. *Nature* **554**, 81–85 (2018).
13. J. A. Jackson, M. C. Messner, N. A. Dudukovic, W. L. Smith, L. Bekker, B. Moran, A. M. Golobic, A. J. Pascall, E. B. Duoss, K. J. Loh, C. M. Spadaccini, Field responsive mechanical metamaterials. *Sci. Adv.* **4**, eaau6419 (2018).
14. Y. Sato, Y. Hiratsuka, I. Kawamata, S. Murata, S.-i. M. Nomura, Micrometer-sized molecular robot changes its shape in response to signal molecules. *Sci. Robot.* **2**, eaal3735 (2017).
15. E. Acome, S. K. Mitchell, T. G. Morrissey, M. B. Emmett, C. Benjamin, M. King, M. Radakovitz, C. Keplinger, Hydraulically amplified self-healing electrostatic actuators with muscle-like performance. *Science* **359**, 61–65 (2018).
16. J. A. Faber, A. F. Arrieta, A. R. Studart, Bioinspired spring origami. *Science* **359**, 1386–1391 (2018).
17. S. Tibbits, 4D printing: Multi-material shape change. *Archit. Des.* **84**, 116–121 (2014).
18. K. Bertoldi, V. Vitelli, J. Christensen, M. van Hecke, Flexible mechanical metamaterials. *Nat. Rev. Mater.* **2**, 17066 (2017).
19. R. F. Shepherd, F. Ilievski, W. Choi, S. A. Morin, A. A. Stokes, A. D. Mazzeo, X. Chen, M. Wang, G. M. Whitesides, Multigait soft robot. *Proc. Natl. Acad. Sci. U.S.A.* **108**, 20400–20403 (2011).
20. A. G. Mark, S. Palagi, T. Qiu, P. Fischer, Auxetic metamaterial simplifies soft robot design, in *Proceedings of the 2016 IEEE International Conference on Robotics and Automation (ICRA)*, Stockholm, Sweden, 16 to 21 May 2016 (IEEE, 2016), pp. 4951–4956.
21. J. I. Lipton, R. MacCurdy, Z. Manchester, L. Chin, D. Cellucci, D. Rus, Handedness in shearing auxetics creates rigid and compliant structures. *Science* **11**, 632–635 (2018).
22. T. Li, Y. Chen, X. Hu, Y. Li, L. Wang, Exploiting negative Poisson's ratio to design 3D-printed composites with enhanced mechanical properties. *Mater. Des.* **142**, 247–258 (2018).
23. T. Li, L. Wang, Bending behavior of sandwich composite structures with tunable 3D-printed core materials. *Compos. Struct.* **175**, 46–57 (2017).
24. J. Shim, C. Perdigou, E. R. Chen, K. Bertoldi, P. M. Reis, Buckling-induced encapsulation of structured elastic shells under pressure. *Proc. Natl. Acad. Sci. U.S.A.* **109**, 5978–5983 (2012).
25. D. Yang, B. Mosadegh, A. Ainla, B. Lee, F. Khashai, Z. Suo, K. Bertoldi, G. M. Whitesides, Buckling of elastomeric beams enables actuation of soft machines. *Adv. Mater.* **27**, 6323–6327 (2015).
26. S. Janbaz, F. S. L. Bobbert, M. J. Mirzaali, A. A. Zadpoor, Ultra-programmable buckling-driven soft cellular mechanisms. *Mater. Horiz.* **6**, 1138–1147 (2019).
27. D. Goswami, S. Liu, A. Pal, L. G. Silva, R. V. Martinez, 3D-architected soft machines with topologically encoded motion. *Adv. Funct. Mater.* **29**, 1808714 (2019).
28. S. Liu, A. I. Azad, R. Burgueño, Architected materials for tailorable shear behavior with energy dissipation. *Extreme Mech. Lett.* **28**, 1–7 (2019).
29. T. Chen, J. Mueller, K. Shea, Integrated design and simulation of tunable, multi-state structures fabricated monolithically with multi-material 3D printing. *Sci. Rep.* **7**, 45671 (2017).
30. H. Yasuda, T. Tachi, M. Lee, J. Yang, Origami-based tunable truss structures for non-volatile mechanical memory operation. *Nat. Commun.* **8**, 962 (2017).
31. Z. Zhao, X. Kuang, J. Wu, Q. Zhang, G. H. Paulino, H. J. Qi, D. Fang, 3D printing of complex origami assemblages for reconfigurable structures. *Soft Matter* **14**, 8051–8059 (2018).
32. M. Zhang, J. Yang, R. Zhu, Flexural wave control via origami-based elastic metamaterials, *Proc. SPIE* **10972**, 109720Q (2019).
33. A. Maziz, A. Concas, A. Khaldi, J. Stålhand, N.-K. Persson, E. W. H. Jager, Knitting and weaving artificial muscles. *Sci. Adv.* **3**, e1600327 (2017).
34. A. Rafsanjani, K. Bertoldi, A. R. Studart, Programming soft robots with flexible mechanical metamaterials. *Sci. Robot.* **4**, eaav7874 (2019).
35. D. Raviv, W. Zhao, C. Mcknelly, A. Papadopoulou, A. Kadambi, B. Shi, S. Hirsch, D. Dikovsky, M. Zyracki, C. Olguin, R. Raskar, S. Tibbits, Active printed materials for complex self-evolving deformations. *Sci. Rep.* **4**, 7422 (2015).
36. L. H. Dudte, E. Vouga, T. Tachi, L. Mahadevan, Programming curvature using origami tessellations. *Nat. Mater.* **15**, 583–588 (2016).
37. J. L. Silverberg, J.-H. Na, A. A. Evans, B. Liu, T. C. Hull, C. D. Santangelo, R. J. Lang, R. C. Hayward, I. Cohen, Origami structures with a critical transition to bistability arising from hidden degrees of freedom. *Nat. Mater.* **14**, 389–393 (2015).
38. S. Miyashita, S. Guitron, S. Li, D. Rus, Robotic metamorphosis by origami exoskeletons. *Sci. Robot.* **2**, eaao4369 (2017).
39. A. Pugh, *An Introduction to Tensegrity* (University of California Press, 1976).
40. C. Sultan, Tensegrity: Sixty years of art, science, and engineering, in *Advances in Applied Mechanics*, H. Aref, E. van der Giessen, Eds. (Elsevier, 2009), vol. 43, chap. 2, pp. 69–145.
41. R. E. Skelton, M. C. de Oliveira, *Tensegrity Systems* (Springer, 2009).
42. R. B. Fuller, Tensile integrity structures. U.S. Patent 3,063,521 (1962).
43. S. Sadao, Fuller on tensegrity. *Int. J. Space Struct.* **11**, 37–42 (1996).
44. D. E. Ingber, Cellular tensegrity: Defining new rules of biological design that govern the cytoskeleton. *J. Cell Sci.* **104**, 613–627 (1993).
45. D. E. Ingber, The architecture of life. *Sci. Am.* **278**, 48–57 (1998).
46. D. E. Ingber, Tensegrity I. Cell structure and hierarchical systems biology. *J. Cell Sci.* **116**, 1157–1173 (2003).
47. F. J. Valero-Cuevas, J.-W. Yi, D. Brown, R. V. McNamara III, C. Paul, H. Lipson, The tendon network of the fingers performs anatomical computation at a macroscopic scale. *IEEE Trans. Biomed. Eng.* **54**, 1161–1166 (2007).
48. G. Scarr, *Biotensegrity: The Structural Basis of Life* (Handspring Publishing, 2014).
49. P. A. Janmey, The cytoskeleton and cell signaling: Component localization and mechanical coupling. *Physiol. Rev.* **78**, 763–781 (1998).
50. R. Motro, Tensegrity systems: The state of the art. *Int. J. Space Struct.* **7**, 75–83 (1992).
51. K. Snelson, The art of tensegrity. *Int. J. Space Struct.* **27**, 71–80 (2012).
52. F. Carreño, M. A. Post, Design of a novel wheeled tensegrity robot: A comparison of tensegrity concepts and a prototype for travelling air ducts. *Robot. Biomim.* **5**, 1 (2018).
53. R. E. Skelton, F. Fraternali, G. Carpentieri, A. Michletti, Minimum mass design of tensegrity bridges with parametric architecture and multiscale complexity. *Mech. Res. Comm.* **58**, 124–132 (2014).
54. Z. Vanik, M. Magura, Modern lightweight structures. *Appl. Mech. Mater.* **824**, 42–49 (2016).
55. P. Polinceusz, Structure of architecture—Tensegrities in the construction of architectural space. *Archit. Civil Eng. Environ.* **12**, 45–52 (2019).
56. Y. Koizumi, M. Shibata, S. Hirai, Rolling tensegrity driven by pneumatic soft actuators, in *Proceedings of the 2012 IEEE International Conference on Robotics and Automation (ICRA)*, Saint Paul, MN, 14 to 18 May 2012 (IEEE, 2012), pp. 1988–1993.
57. K. Kim, A. K. Agogino, D. Moon, L. Teneja, A. Toghyan, B. Dehghani, V. SunSpiral, A. M. Agogino, Rapid prototyping design and control of tensegrity soft robot for locomotion, in *Proceedings of the 2014 IEEE International Conference on Robotics and Biomimetics (ROBIO 2014)*, Bali, Indonesia, 5 to 10 December 2014 (IEEE, 2014), pp. 7–14.
58. K. Caluwaerts, J. Despraz, A. Işçen, A. P. Sabelhaus, J. Bruce, B. Schrauwen, V. SunSpral, Design and control of compliant tensegrity robots through simulation and hardware validation. *J. R. Soc. Interface* **11**, 20140520 (2014).
59. A. Melnyk, A. Pitti, Synergistic control of a multi-segments vertebral column robot based on tensegrity for postural balance. *Adv. Robot.* **32**, 850–864 (2018).
60. E. Jung, V. Ly, N. Cessna, M. L. Ngo, D. Castro, V. SunSpiral, M. Teodorescu, Bio-inspired tensegrity flexural joint, in *Proceedings of the 2018 IEEE International Conference on Robotics and Automation (ICRA)*, Brisbane, Australia, 21 to 25 May 2018 (IEEE, 2018), pp. 1–6.
61. F. Fraternali, G. Carpentieri, A. Amendola, R. E. Skelton, V. F. Nesterenko, Multiscale tunability of solitary wave dynamics in tensegrity metamaterials. *Appl. Phys. Lett.* **105**, 201903 (2014).
62. X.-F. Yuan, S. Ma, S.-H. Jiang, Form-finding of tensegrity structures based on the Levenberg–Marquardt method. *Comput. Struct.* **192**, 171–180 (2017).
63. A. Al Sabouni-Zawadzka, W. Gilewski, Soft and stiff simplex tensegrity lattices as extreme smart metamaterials. *Materials* **12**, 187 (2019).
64. K. Liu, G. H. Paulino, Tensegrity topology optimization by force maximization on arbitrary ground structures. *Struc. Multidiscip. Optim.* **59**, 2041–2062 (2019).
65. K. Liu, J. Wu, G. H. Paulino, H. J. Qi, Programmable deployment of tensegrity structures by stimulus-responsive polymers. *Sci. Rep.* **7**, 3511 (2017).
66. M. Shibata, F. Saijyo, S. Hirai, Crawling by body deformation of tensegrity structure robots, in *Proceedings of the 2009 IEEE International Conference on Robotics and Automation (ICRA)*, Kobe, Japan, 12 to 17 May 2009 (IEEE, 2009), pp. 4375–4380.
67. Z. Wang, K. Li, Q. He, S. Cai, A light-powered ultralight tensegrity robot with high deformability and load capacity. *Adv. Mater.* **31**, 1806849 (2019).
68. L. Wu, M. Jung de Andrade, T. Brahme, Y. Tadesse, R. H. Baughman, A reconfigurable robot with tensegrity structure using nylon artificial muscle, *Proc. SPIE* **9799**, 97993K (2016).
69. D. Zappetti, S. H. Jeong, J. Shintake, D. Floreano, Phase changing materials-based variable-stiffness tensegrity structures. *Soft Robot.* **7**, 362–369 (2020).
70. D. Zappetti, S. Mintchev, J. Shintake, D. Floreano, M. Mangan, M. Cutkosky, A. Mura, P. Verschure, T. Prescott, N. Lepora, Bio-inspired tensegrity soft modular robots, in *Proceedings of the Bio-inspired Tensegrity Soft Modular Robots BT - Biomimetic and Biohybrid Systems: 6th International Conference Living Machines 2017*, Stanford, CA, 26 to 28 July 2017 (Springer International Publishing, 2017), pp. 497–508.
71. S. Mintchev, D. Zappetti, J. Willemin, D. Floreano, Soft robot for random exploration of terrestrial environments, in *Proceedings of the 2018 IEEE International Conference on Robotics and Automation (ICRA)*, Brisbane, Australia, 21 to 25 May 2018 (IEEE, 2018), pp. 7492–7497.
72. J. Kim, S. E. Chung, S.-E. Choi, H. Lee, J. Kim, S. Kwon, Programming magnetic anisotropy in polymeric microactuators. *Nat. Mater.* **10**, 747–752 (2011).

73. S. Jeon, S. Kim, S. Ha, S. Lee, E. Kim, S. Y. Kim, S. H. Park, J. H. Jeon, S. W. Kim, C. Moon, B. J. Nelson, J.-y. Kim, S.-W. Yu, H. Choi, Magnetically actuated microrobots as a platform for stem cell transplantation. *Sci. Robot.* **4**, eaav4317 (2019).
74. T. Xu, J. Zhang, M. Salehizadeh, O. Onaizah, E. Diller, Millimeter-scale flexible robots with programmable three-dimensional magnetization and motions. *Sci. Robot.* **4**, eaav4494 (2019).
75. Y. Kim, H. Yuk, R. Zhao, S. A. Chester, X. Zhao, Printing ferromagnetic domains for untethered fast-transforming soft materials. *Nature* **558**, 274–279 (2018).

Funding: We acknowledge the financial support from the Basic Science Research Program (NRF-2017R1D1A1B03034297) and the Leading Foreign Research Institute Recruitment Program (2017K1A4A3015437) through the National Research Foundation of Korea (NRF) funded by the Ministry of Science and ICT (MSIP) of the Republic of Korea; the Industrial Strategic Technology Development Program supervised by the Korea Evaluation Institute of Industrial Technology (KEIT) funded by the Ministry of Trade, Industry and Energy (MOTIE) of the Republic of Korea (20009103); and the Research funds of UNIST [Ulsan National Institute of Science and Technology (1.180059.01, 1.160107.01, and 1.200095.01)]. **Author contributions:** J.K. and H.L. conceived the idea of smart tensegrity as a design principle for smart architecture. J.K. and H.L. designed the experiments. H.L. fabricated structures and demonstrated their functions. H.L. and J.K.C. measured mechanical properties of flexible tendon component. J.K.C. simulated mechanical properties of tensegrity beams. Y.J. developed starfish robot driving system. J.K., H.L., Y.J., H.S., S.L., J.P.L., and N.L. generated figures and the Supplementary Materials. J.K. and H.L. interpreted results and wrote the manuscript with input from all authors. J.K. supervised the study. **Competing interests:** The authors declare that they have no competing interests. **Data and materials availability:** All data necessary to evaluate the conclusions of the paper are provided in the paper or the Supplementary Materials.

Submitted 11 September 2019
Accepted 3 August 2020
Published 26 August 2020
10.1126/scirobotics.aay9024

Citation: H. Lee, Y. Jang, J. K. Choe, S. Lee, H. Song, J. P. Lee, N. Lone, J. Kim, 3D-printed programmable tensegrity for soft robotics. *Sci. Robot.* **5**, eaay9024 (2020).

Science Robotics

3D-printed programmable tensegrity for soft robotics

Hajun Lee, Yeonwoo Jang, Jun Kyu Choe, Suwoo Lee, Hyeonseo Song, Jin Pyo Lee, Nasreena Lone, and Jiyun Kim

Sci. Robot. **5** (45), eaay9024. DOI: 10.1126/scirobotics.aay9024

Science Robotics (ISSN 2470-9476) is published by the American Association for the Advancement of Science. 1200 New York Avenue NW, Washington, DC 20005. The title *Science Robotics* is a registered trademark of AAAS.